oping better parallel assembly schemes for nanowire integration (*29*).

References and Notes

1. S. Noda, K. Tomoda, N. Yamamoto, A. Chutinan, *Science* **289**, 604 (2000).
2. C. López, *Adv. Mater.* **15**, 1679 (2003).
3. W. L. Barnes, A. Dereux, T. W. Ebbesen, *Nature* **424**, 824 (2003).
4. J. R. Krenn, J.-C. Weeber, *Philos. Trans. R. Soc. Lond. A* **362**, 739 (2004).
5. X. Duan *et al.*, *Nature* **425**, 274 (2003).
6. M. C. McAlpine *et al.*, *Nano Lett.* **3**, 1531 (2003).
7. M. H. Huang *et al.*, *Science* **292**, 1897 (2001).
8. X. Duan, Y. Huang, R. Agarwal, C. M. Lieber, *Nature* **421**, 241 (2003).
9. H. Kind, H. Yan, B. Messer, M. Law, P. Yang, *Adv. Mater.* **14**, 158 (2002).
10. D. Psaltis, *Science* **298**, 1359 (2002).
11. P. Yang *et al.*, *Science* **287**, 465 (2000).
12. R. Quidant *et al.*, *Phys. Rev. E* **64**, 066607 (2001).
13. V. R. Almeida, Q. Xu, C. A. Barrios, M. Lipson, *Opt. Lett.* **29**, 1209 (2004).
14. L. Tong *et al.*, *Nature* **426**, 816 (2003).
15. M. Law, H. Kind, B. Messer, F. Kim, P. Yang, *Angew. Chem. Int. Ed. Engl.* **41**, 2405 (2002).
16. H. Yan *et al.*, *Adv. Mater.* **15**, 1907 (2003).
17. Z. W. Pan, Z. R. Dai, Z. L. Wang, *Science* **291**, 1947 (2001).
18. Materials and methods are available as supporting material on *Science* Online.
19. C. Gmachl *et al.*, *Science* **280**, 1556 (1998).
20. A. W. Snyder, D. Love, *Optical Waveguide Theory* (Kluwer, Boston, 1983).
21. We also have observed extremely convoluted "wet noodle" shapes in the case of thin (<50 nm) non-waveguiding nanoribbons dispersed on surfaces, including loops with radii of 100 nm.
22. H. W. C. Postma, A. Sellmeijer, C. Dekker, *Adv. Mater.* **12**, 1299 (2000).
23. K. Kim *et al.*, *Rev. Sci. Instrum.* **74**, 4021 (2003).
24. J. C. Johnson, H. Yan, P. Yang, R. J. Saykally, *J. Phys. Chem. B* **107**, 8816 (2003).
25. R. C. Reddick, R. J. Warmack, D. W. Chilcott, S. L. Sharp, T. L. Ferrell, *Rev. Sci. Instrum.* **61**, 3669 (1990).
26. K. Okamoto, *Fundamentals of Optical Waveguides* (Academic Press, San Diego, CA, 2000).
27. L. Eldada, *Rev. Sci. Instrum.* **75**, 575 (2004).
28. H. J. Egelhaaf, D. Oelkrug, *J. Cryst. Growth* **161**, 190 (1996).
29. A. Tao *et al.*, *Nano Lett.* **3**, 1229 (2003).
30. This work was supported in part by the Camille and Henry Dreyfus Foundation, the Alfred P. Sloan Foundation, the Beckman Foundation, the U.S. Department of Energy, and NSF. J.G. thanks NSF for a graduate research fellowship. Work at the Lawrence Berkeley National Laboratory was supported by the Office of Science, Basic Energy Sciences, Division of Materials Science of the U. S. Department of Energy. We thank H. Yan for the ZnO nanowires and the National Center for Electron Microscopy for the use of their facilities.

Transparent, Conductive Carbon Nanotube Films

Zhuangchun Wu,[1]* Zhihong Chen,[1]*† Xu Du,[1]
Jonathan M. Logan,[1] Jennifer Sippel,[1] Maria Nikolou,[1]
Katalin Kamaras,[2] John R. Reynolds,[3] David B. Tanner,[1]
Arthur F. Hebard,[1] Andrew G. Rinzler[1]‡

We describe a simple process for the fabrication of ultrathin, transparent, optically homogeneous, electrically conducting films of pure single-walled carbon nanotubes and the transfer of those films to various substrates. For equivalent sheet resistance, the films exhibit optical transmittance comparable to that of commercial indium tin oxide in the visible spectrum, but far superior transmittance in the technologically relevant 2- to 5-micrometer infrared spectral band. These characteristics indicate broad applicability of the films for electrical coupling in photonic devices. In an example application, the films are used to construct an electric field–activated optical modulator, which constitutes an optical analog to the nanotube-based field effect transistor.

Transparent electrical conductors pervade modern technologies, providing a critical component of video displays, video and still-image recorders, solar cells, lasers, optical communication devices, and solid-state lighting [for recent reviews, see (*1*, *2*)]. We describe a class of transparent conducting material based on continuous films of pure single-walled carbon nanotubes (SWNTs). These intrinsic electrical conductors are formed into uniform, optically homogeneous films of controllable thickness that are thin enough to be transparent over technologically relevant regions of the electromagnetic spectrum. Use of the transparent SWNT films (t-SWNTs) for current injection into p-GaN and for blue light–emitting GaN/InGaN diodes (light extracted through the films) has recently been demonstrated, together with patterning of the t-SWNTs by standard microlithographic techniques (*3*). Here we elaborate on the film production process, transfer to substrates, film morphology, and electrical and optical properties. We also demonstrate use of the t-SWNTs as the active element of an optical modulator. This constitutes an optical analog to the SWNT-based field-effect transistor (FET), modulating light transmission through the films by application of electric fields.

Other methods of transparent nanotube film production include drop-drying from solvent, airbrushing, and Langmuir-Blodgett deposition. These alternatives, however, present severe limitations in terms of the film quality or production efficiency (*4*). Our t-SWNT production process is quite simple, comprising three steps: (i) vacuum-filtering a dilute, surfactant-based suspension of purified nanotubes onto a filtration membrane (forming the homogeneous film on the membrane); (ii) washing away the surfactant with purified water; and (iii) dissolving the filtration membrane in solvent (*4*). Multiple techniques for transfer of the film to the desired substrate have been developed. The films can be made free-standing over appreciable apertures (~1 cm²) by making the transfer to a substrate with a hole, over which the film is laid before membrane dissolution (*5*, *6*).

This filtration method has several advantages: (i) Homogeneity of the films is guaranteed by the process itself. As the nanotubes accumulate, they generate a filter cake that acts to impede the permeation rate. If a region becomes thicker, the local permeation rate and associated deposition rate slow down, allowing thinner regions to catch up. (ii) Because of their extreme rigidity (for objects of such small diameters), the nanotubes have long persistence lengths. They consequently tend to lie straight, gaining maximal overlap and interpenetration within the film as they accumulate (the curvature observed in Fig. 1D is likely caused by van der Waals forces dominating as the surfactant is washed away). This yields maximal electrical conductivity and mechanical integrity throughout the films. (iii) The film thickness is readily controlled, with nanoscale precision, by the nanotube concentration and volume of the suspension filtered.

Examples of the transparent films are shown in Fig. 1. Films of thickness 50 and 150 nm, as measured by atomic force microscopy (AFM) at step edges, display a corresponding increase in optical density (Fig. 1A). Films as large as 10 cm in diam-

Departments of ¹Physics and ³Chemistry, University of Florida, Gainesville, FL 32611, USA. ²MTA SzFKI, Budapest, H 1525, Hungary.

*These authors contributed equally to this work.
†Present address: IBM T. J. Watson Research Center, Yorktown Heights, NY 10598, USA.
‡To whom correspondence should be addressed. E-mail: rinzler@phys.ufl.edu

eter have been fabricated (Fig. 1B), but they could readily be made larger still. Film size is ultimately limited only by the dimensions of the filtration membranes, which are available in rolls as large as 30 cm by 10 m (Millipore). The t-SWNTs are highly flexible (Fig. 1C), with no observed degradation in their conductance after repeated flexure. Figure 1D shows the AFM image of a transparent nanotube film surface. The t-SWNTs have nanoscale porosity; however, for thicknesses greater than ~50 nm there are few straight, unobstructed paths through the network.

Figure 2 shows the transmittance spectrum for a 240-nm-thick, free-standing film over a broad spectral range and that for a 50-nm-thick film (on quartz) over a more limited range. The nanotubes are charge transfer–doped (acceptor-doped) by the nitric acid treatment used in their purification (7, 8). This depletes electrons from valence-band van Hove singularities (see inset), reducing the rate of electronic transitions responsible for the absorption bands labeled S1, S2, and M1 (9). Heating the films to 600°C in inert gas desorbs the dopant, yielding the curves in which these absorption intensities are maximized (black curves). The transmittance going toward the far-infrared (IR) is limited by free carrier absorption (7). Such assignment is consistent with the lower transmittance in the mid-IR for the unbaked (hole-doped) film and with the increased transmittance there accompanying the loss of free carriers upon baking (dedoping). The as-prepared 50-nm film has transmittance greater than 70% over the visible part of the spectrum. In the near-IR at 2 μm, this film has transmittance greater than 90%. Use of Beer's law to scale the transmittance of the (unbaked) 240-nm film to a thickness of 50 nm indicates that the transmittance should remain >90% to just beyond 5 μm. Hence, such a film can be anticipated to have a window of >90% transmittance in a 2- to 5-μm spectral band.

The sheet resistance of the as-prepared 50-nm film was measured to be 30 ohm/ square (resistivity 1.5×10^{-4} ohm·cm). Given the lack of index-matching antireflection coatings, this is a remarkably high transmittance for such low sheet resistance. For comparison purposes, the state-of-the-art mixed-oxide spinel $Ni_xCo_{x-1}O_{3/4}$ is more resistive (resistivity 3×10^{-3} ohm·cm) with a lower transmittance of 78% at 5 μm, achieved only after correcting for reflection losses, which is necessary because of the high refractive index of the material (10). Dedoped (baked) films are more transmissive further into the IR at the expense of some transmittance in the visible, and have resistivity about an order of

magnitude higher than that of as-prepared, unbaked films. Note that the as-prepared films are not maximally doped, hence the 30 ohm/square sheet resistance does not represent a lower limit.

For transparent conductors, the plasma frequency marks the onset of high IR reflection. The dependence of the plasma frequency on carrier density, which also plays a critical role in the material's conductivity, results in a trade-off between conductivity and IR transparency. Much of the extensive research effort in traditional transparent conducting oxides focuses on changing the oxygen content or impurity doping during growth to modify the carrier concentration. The window of transparency is thereby optimized to

the target spectral region while minimizing any trade-off in decreased conductivity. For the nanotubes, the ease of chemical charge-transfer doping to obtain such transparency-versus-conductivity optimization (via exposure of the nanotubes to vapors of appropriate chemicals) provides an additional advantage for the t-SWNTs. Moreover, charge transport in these t-SWNTs is p-type, unlike the far more common transparent conducting oxides [e.g., indium tin oxide (ITO)], which are n-type. This should permit new complementary applications and alternative photonic coupling schemes (3).

Chemical charge-transfer doping, which adds or removes electrons from the nanotubes, shifts their Fermi levels. Such
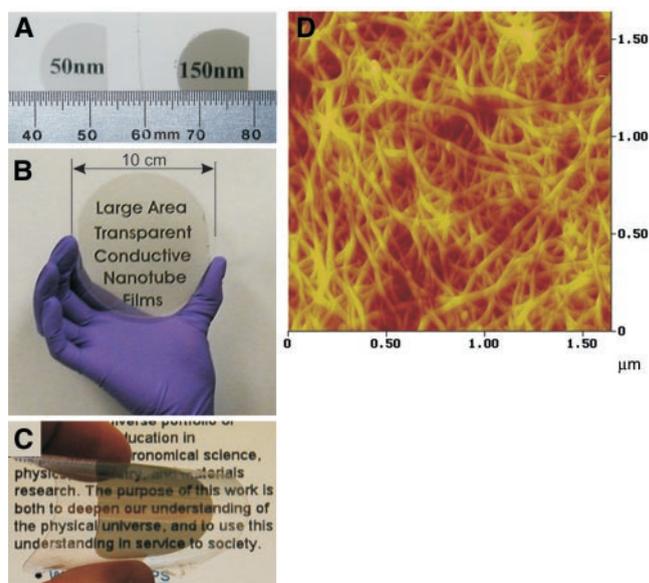
Fig. 1. Transparent SWNT films. (**A**) Films of the indicated thickness on quartz substrates. (**B**) A large, 80-nm-thick film on a sapphire substrate 10 cm in diameter. (**C**) Flexed film on a Mylar sheet. (**D**) AFM image of a 150-nm-thick t-SWNT film surface (color scale: black to bright yellow, 30 nm). The text in (A) to (C) lies behind the films.
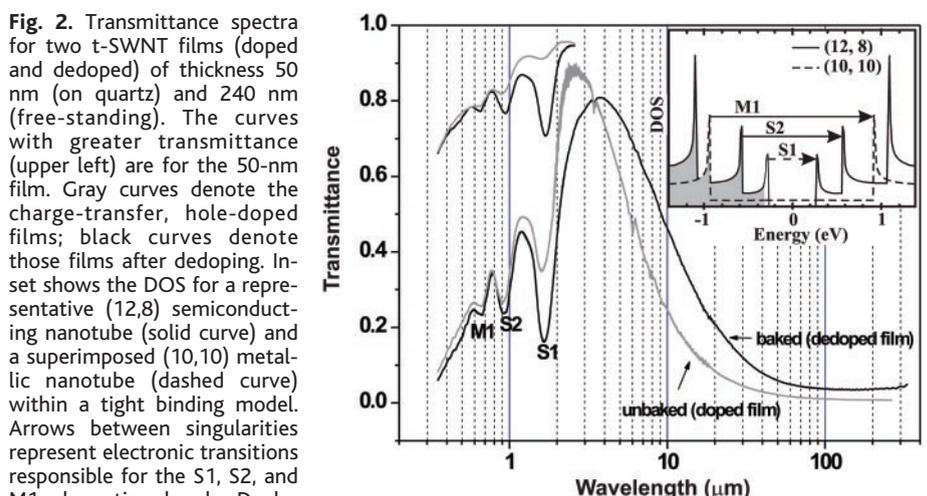
Fig. 2. Transmittance spectra for two t-SWNT films (doped and dedoped) of thickness 50 nm (on quartz) and 240 nm (free-standing). The curves with greater transmittance (upper left) are for the 50-nm film. Gray curves denote the charge-transfer, hole-doped films; black curves denote those films after dedoping. Inset shows the DOS for a representative (12,8) semiconducting nanotube (solid curve) and a superimposed (10,10) metallic nanotube (dashed curve) within a tight binding model. Arrows between singularities represent electronic transitions responsible for the S1, S2, and M1 absorption bands. Depletion of the first singularity (filled electronic states in gray) results in the loss of the corresponding electronic transition (dashed arrow) and loss of the associated S1 absorption intensity. The t-SWNT films consist of a mixture of semiconducting and metallic nanotubes with a distribution of diameters and chiral angles. The (n,m) index dependence of the spacing between van Hove singularities modulates the transition energies to yield the broad absorption bands seen in the spectra (also labeled S1, S2, and M1). Bundling of the nanotubes further broadens the observed absorption bands.

Fermi level shifts need not be induced chemically; they can also be induced by electric fields. In a nanotube-based FET (NFET), a semiconducting nanotube is electrically coupled to source and drain terminals while the field between the nanotube and an isolated gate electrode shifts the nanotube Fermi level, modulating its carrier concentration (11–14). In an electrolyte-gated NFET, the gate electrode is provided by an electrolyte in contact with a remote electrode (15, 16). Applying a potential between the nanotube (via the source/drain terminals) and the remote electrode establishes an electric double layer consisting of the excess charge drawn onto the nanotube from the source/drain terminals compensated by the near-lying cloud of oppositely charged electrolyte ions. As long as the gate voltage is kept below potentials at which redox reactions occur, the ionic cloud of the electric double layer behaves like an exceptionally near-lying gate electrode.
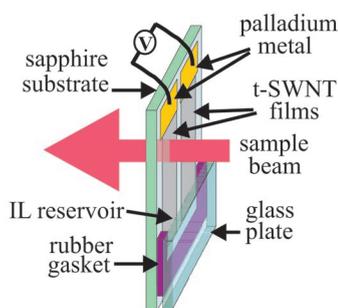
Figure 3 shows a device schematic that constitutes an optical analog to the electrolyte-gated NFET—that is, it modulates light transmission through the device as a function of the electrolyte "gate" potential (17). The device consists of two adjacent t-SWNT films (each 150 nm thick) deposited onto a sapphire substrate. For electrical contact, each film has palladium metal (18) sputtered across one end. A U-shaped rubber gasket between the bottom portion of the substrate and a glass plate forms a reservoir into which the non–metal-coated end of each t-SWNT film extends (a clamp holding the plates together is not shown). While they are positioned horizontally, the films are saturated with the ionic liquid (IL) 1-ethyl-3-methylimidazolium bis(trifluoromethylsulfonyl)imide. When the assembly is tipped up to lie vertically, excess IL drains into the reservoir. Because the IL wets the nanotubes, a thin layer, bridged by the IL drained into the reservoir, remains associated with each film. Monochromatic light from the sample beam of a Perkin-Elmer Lamba 900 spectrophotometer is passed through only one of the SWNT films. The second film provides a "gating" counterelectrode with nanoscale surface area comparable to that of the optically probed film. A counterelectrode with smaller surface area would limit the capacitance, decreasing the charging efficiency of the probed film. The density of electronic states (DOS) for the nanotubes (Fig. 2, inset) illustrates the idea behind the device. A negative potential applied to the gating (counterelectrode) film depletes electrons from the van Hove singularity associated

with the S1 electronic transitions for the probed film. This results in a loss of the corresponding absorption and increased optical transmission through the device at the associated wavelength.

Figure 4 shows the optical transmittance for the optical NFET (O-NFET) illustrated in Fig. 3 as a function of voltage applied between the films. At the S1 absorbance maximum (1676 nm), the transmittance is modulated from 44% to 92% between "gate" (counterelectrode) potentials of ±1.8 V (19–23). Further in the IR at 3080 nm, the modulation is from 97% to 75% over the same voltage range. Relative to the changes in the S1, S2, and M1 bands, transmittance changes at wavelengths greater than ~2000 nm occur in the opposite direction with voltage. Negative counterelectrode potentials draw excess holes onto the probed film, increasing the free carrier absorption and reducing the transmission, whereas positive counterelectrode potentials reduce the hole concentration, decreasing the free carrier absorption and increasing the transmission. These modulations in the transmittance are fully reversible, with no degradation observed after hundreds of cycles (24).

For the S1, S2, and M1 absorbance bands, the SWNT DOS (Fig. 2, inset) would suggest a symmetry between positive and negative applied potentials. Negative gate potentials should deplete the initial transition-state (valence band) singularities, decreasing the absorption intensities. Positive gate potentials should fill the terminal-state (conduction band) singularities. With fewer terminal states available

Fig. 3. Optical analog to the electrolyte-gated NFET (O-NFET).
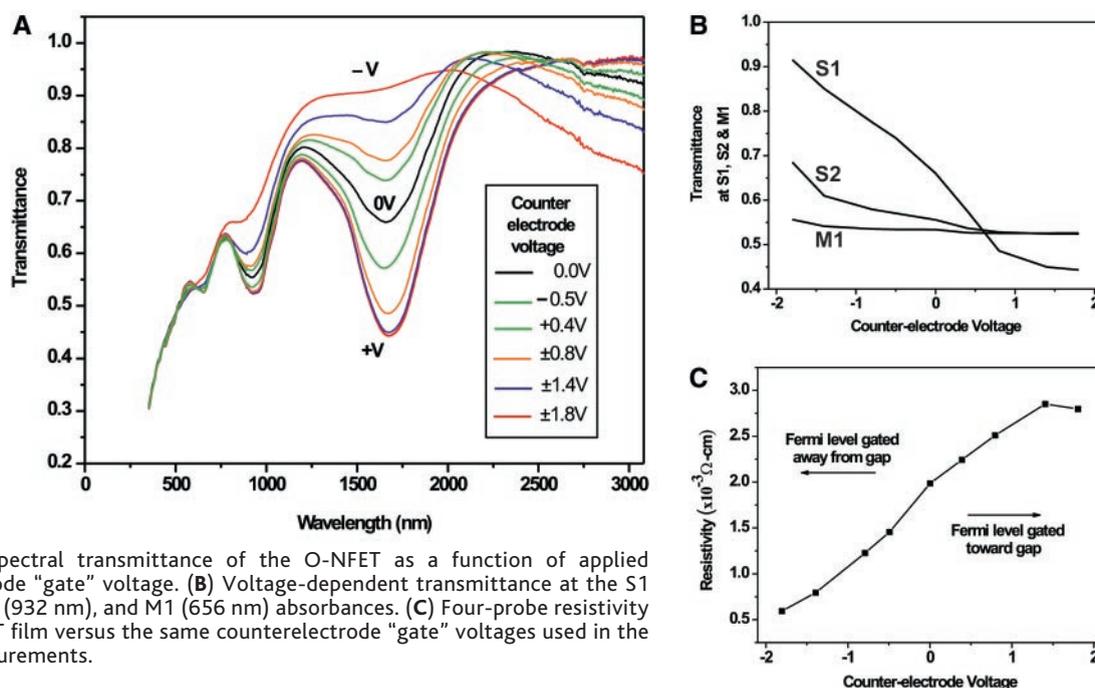
Fig. 4. (**A**) Spectral transmittance of the O-NFET as a function of applied counterelectrode "gate" voltage. (**B**) Voltage-dependent transmittance at the S1 (1676 nm), S2 (932 nm), and M1 (656 nm) absorbances. (**C**) Four-probe resistivity of the t-SWNT film versus the same counterelectrode "gate" voltages used in the spectral measurements.

1275

for the transition, this should also decrease the absorption intensities. The corresponding behavior in an electronic NFET has the Fermi level lying in the gap and the conductance increasing for both positive and negative gate potentials, in which case the device is said to be ambipolar. The zero voltage curve for the O-NFET does not yield the maximum absorption intensities for the S1, S2, and M1 bands, as would be expected for the intrinsic Fermi level lying in the gap. Rather, positive gate voltages increase those absorption intensities, whereas negative gate voltages decrease those intensities. This p-doped–like behavior (which has the Fermi level of the semiconducting nanotubes underlying the S1 valence singularity at 0 V) appears despite the films having been dedoped (baked) before saturation of the t-SWNT films with the ionic liquid. One possible explanation for this seemingly intrinsic p-type behavior is equilibration of the chemical potentials among the nanotubes, the Pd electrodes, and the ionic liquid. Alternatively, impurities in the ionic liquid may lead to chemical charge-transfer doping of the nanotubes.

The simple model provided by the DOS (Fig. 2, inset) further suggests that the changes in the S1, S2, and M1 absorbance intensities should emerge sequentially as the Fermi level progresses sequentially through the corresponding valence band singularities. That is, changes in S1 should be complete before changes in S2 begin, followed (once the latter has been fully saturated) by changes in M1. As seen in Fig. 4B, which plots the transmittance at the S1, S2, and M1 absorbance peaks against the gate potentials, the changes in transmittance there clearly do not arise sequentially. This apparent inconsistency is explained by the fact that the nanotubes are bundled together in hexagonal close packing that excludes the large ionic liquid ions from the interiors of the bundles. With applied potential, ions of the double layer attract electronic countercharges to the outermost nanotubes of the bundles; these charges in turn partially screen the interior nanotubes from the ionic fields. Hence, for a given potential under the electrostatic equilibrium established, the Fermi level for nanotubes on the exterior of a bundle can lie below the M1 valence singularity while that for the interior nanotubes can still lie within the S1 valence singularity. However, the low carrier density of the nanotubes makes their screening less than perfect, so that the S1 singularity—even for the interior nanotubes—can be nearly fully depleted, as indicated by the near-complete loss of the S1 absorption at the counterelectrode potential of –1.8 V.

We have also measured the four-probe resistivity of the t-SWNT films, while they are gated by the counterelectrode, at the potentials used in the optical transmittance measurements (25). When resistivity is plotted against gate voltage (Fig. 4C), the change in resistivity is consistent with a diminished carrier concentration as the Fermi level is gated toward the gap of the semiconducting nanotubes with increasing positive gate voltage. The saturation beyond 1.4 V corresponds to the semiconducting nanotubes no longer contributing to transport through the film. This behavior is also consistent with the saturation appearing in the S1 optical absorption intensity between 1.4 and 1.8 V; once the Fermi level for all the semiconducting nanotubes lies in the gap, the absorbance has already been maximized.

The simultaneous high transparency and good electrical conductivity of the t-SWNTs can be understood on the basis of three properties of the nanotubes: (i) low carrier density; (ii) high electronic mobility; and (iii) the suppression of light absorption and reflection for polarization components perpendicular to the nanotube axis, which reduces the optical density of the disordered SWNT films for unpolarized incident light. Such films are likely to find application as transparent conductors in the IR, where our measurements show them to have exceptional properties. It is too early to tell if they can compete in the visible part of the spectrum against ITO. Given their flexibility, however (ITO is comparatively brittle), they seem likely to at least find niche applications in, e.g., flexible/foldable displays. Devices like our O-NFET optical modulator may find application in spacecraft thermal control and military camouflage countermeasures (26).

References and Notes

1. D. Ginley et al., Mater. Res. Soc. Symp. Proc. **668**, H 2.7.1 (2001).
2. R. G. Gordon, MRS Bull. **25**, 52 (2000).
3. K. Lee et al., Nano Lett. **4**, 911 (2004).
4. See supporting text on Science Online.
5. Others have also used vacuum filtration as the initial step to fabricate free-standing SWNT films (6). However, their transfer process involved cutting a rectangular hole in adhesive tape, laying this tape onto the nanotube layer on the membrane, and peeling up the tape to obtain the free-standing film within the hole in the tape. This gives comparatively little control over the film thickness and is not amenable to film deposition over large areas compatible with microelectronic processing.
6. F. Hennrich et al., Phys. Chem. Chem. Phys. **4**, 2273 (2002).
7. M. E. Itkis et al., Nano Lett. **2**, 155 (2002).
8. F. Hennrich, R. Wellmann, S. Malik, S. Lebedkin, M. M. Kappes, Phys. Chem. Chem. Phys. **5**, 178 (2003).
9. S. Kazaoui, N. Minami, R. Jacquemin, H. Kataura, Y. Achiba, Phys. Rev. B **60**, 13339 (1999).
10. C. F. Windisch Jr., K. F. Ferris, G. J. Exarhos, S. K. Sharma, Thin Solid Films **420–421**, 89 (2002).
11. S. J. Tans, R. M. Verschueren, C. Dekker, Nature **393**, 49 (1998).
12. Work over recent years has shown that this simple picture for NFET operation is by no means complete and ignores Schottky barriers that develop at the nanotube-metal contact junctions, which are also modulated by the gate fields (13). Nonetheless, carrier concentration modulation contributes to the effect and under some conditions dominates (14).
13. S. Heinze et al., Phys. Rev. Lett. **89**, 106801 (2002).
14. A. Javey, J. Guo, Q. Wang, M. Lundstrom, H. Dai, Nature **424**, 654 (2003).
15. M. Kruger, M. R. Buitelaar, T. Nussbaumer, C. Schonenberger, L. Forro, Appl. Phys. Lett. **78**, 1291 (2001).
16. S. Rosenblatt et al., Nano Lett. **2**, 869 (2002).
17. We have also fabricated entirely solid-state devices consisting of a transparent ITO counterelectrode separated from the t-SWNT film by a thin AlO_x dielectric layer.
18. D. Mann, A. Javey, J. Kong, Q. Wang, H. Dai, Nature **424**, 654 (2003).
19. Modulation of the three principal SWNT absorption bands in a three-terminal electrochemical cell has been reported (20, 21). There, the effect was ascribed to nanotube Fermi level shifts associated with intercalated species generated by electrochemical redox reactions in the electrolyte. The SWNT film (produced by airbrushing) used in those experiments evidently did not have sufficient intrinsic conductivity to be used without a thin, transparent platinum electrode (20) or ITO electrode (21) onto which the nanotubes were sprayed. The ionic liquid in our experiments acts merely as a near-lying gate electrode undergoing no complicating redox reactions. It also yields substantially cleaner SWNT spectra over broader voltage and spectral ranges. The spectra we show are raw data.
20. S. Kazaoui, N. Minami, N. Matsuda, H. Kataura, Y. Achiba, Appl. Phys. Lett. **78**, 3433 (2001).
21. L. Kavan et al., J. Phys. Chem. B **105**, 10764 (2001).
22. Although the S1 band overlaps the 1.55-μm wavelength important in optical communications, the ionic liquid–gated device (or any electrolyte-gated device) is far too slow to be useful for modulation at the rates needed in communication devices. Because of the high viscosity of the ionic liquid, the time scale for electrostatic gate equilibration is on the order of minutes.
23. Our all–solid-state device has similar spectral behavior with "gate" voltage; however, the magnitude of the modulation is much smaller (0.2% over ±6 V at the peak of S1) because electrostatic screening allows only the layer of nanotubes nearest the ITO counterelectrode to participate. Because gating is all electronic (as opposed to ionic), however, the response time is much faster than the ionic liquid device.
24. With the spectrophotometer in a mode that records the transmittance at fixed wavelength as a function of time, we sat on the peak of the S1 absorption band while driving the O-NFET with a square wave potential. No systematic changes in the amplitude of the modulation were observed over multiple measurements totaling several hundred cycles. Only small changes (a few percent) in the average transmittance, both up and down, were seen—entirely consistent with spectrometer drift over the long time scale of these measurements.
25. Four-probe measurements were performed with a Linear Research 700 resistance bridge using 2-mV excitation at 16 Hz.
26. P. Chandrasekhar et al., Synth. Metals **135–136**, 23 (2003).
27. Supported by the U.S. Army through Center for Materials in Sensors and Actuators grant DAAD19-00-1-0002 (J.R.R., D.B.T., A.F.H., A.G.R.), NSF grants DMR 0101856 (A.F.H.) and ECS-0210574 (A.G.R.), and NSF-MTA-OTKA international grants 021, N31622 (D.B.T., K.K.), NSF-INT-9902050 (D.B.T., K.K.), and OTKA 034198 (K.K.).